Multiphase Flow Properties of Fractured Geothermal Rocks

Chih-Ying Chen and Roland N. Horne

Stanford Geothermal Program, Stanford University, Stanford, California 94305, USA

alnchen@stanford.edu; horne@stanford.edu

Keywords: relative permeability, multiphase flow, tortuosity, flow structure, flow pattern

ABSTRACT

The understanding of the properties of two-phase flow in fractured rocks is central to the prediction of geothermal reservoir performance. In this study, we suggest an alternative approach to describe the two-phase relative permeability behavior in rough-walled fractures based on the two-phase flow structures. This approach lumps the microscale physical mechanism (viscous and capillary forces) into an apparent observable parameter, *channel tortuosity*, which was found to dominate the reduction of the relative permeabilities from the values that would be expected based on the X-curve. Three artificial fractures, smooth-walled, homogeneously rough-walled and randomly rough-walled fractures, were studied to represent distinct surface geometry and heterogeneity. The experimental results from these three fractures could be described successfully by the proposed model. Furthermore, we found that the magnitude of the channel tortuosity increases when the heterogeneity of the fracture surface increases. Although only three simplified fractures were studied and the relationship between the flow-based heterogeneity and the channel tortuosity is not fully developed yet, we were able to derive an empirical, tortuous channel model generalized from all channel tortuosities from these three fractures. This model can represent the current experimental data and as well as observations from earlier studies with good agreement.

1. INTRODUCTION

Rock fractures or joints often form high-permeable flow pathways and therefore dominate single- or multiphase fluid transports in fractured porous media in geothermal reservoirs. Multiphase flows in fractured media are of great importance and engineering interest in geothermal development and environmental protection. In the last two decades, single-phase flow in fractures has been widely studied experimentally, numerically and theoretically. Several models have been proposed to describe the single-phase hydraulic properties in rough fractures (Witherspoon et al., 1980; Zimmerman and Bodvarsson, 1996; Meheust and Schmittbuhl, 2001; Lomize, 1951). However, limited studies have been done to determine the fundamentals of multiphase flow behavior in fractures, especially the effects of fracture geometry on relative permeabilities.

Chen et al. (2004a) suggested a phenomenological approach, the tortuous channel approach (TCA), to describe the air-water relative permeability behavior in a smooth-walled fracture. A method to evaluate the mutual tortuosities induced by the blocking phase, namely the *channel tortuosity*, was proposed from observations of the flow structure images. With verification from laboratory experiments and visualizations, it was concluded that in smooth-walled fractures the coefficients of channel

tortuosity dominate the reduction of the relative permeability values from the X-curve (i.e. relative permeability equals saturation). The results also indicated that the X-curve relative permeability cannot be reached for two-phase flows in fractures even if their surfaces are smooth. Instead, an upper bound for the air-water relative permeability in fractures was proposed. Despite the successful representation of the experimental results in the smooth-walled fracture, the feasibility of using TCA to describe the relative permeabilities in rough fractures was not studied – the rough-walled fracture represents a flow configuration much close to that expected in real rocks.

This research extended and modified the TCA to include rough-walled fractures. Existing and newly measured experimental data from two rough fractures with distinct surface roughness, randomly rough (RR) and homogeneously rough (HR), were used to evaluate and generalize this modified approach. Finally, a more general model deduced from these data was proposed to describe two-phase relative permeabilities in both smooth and rough fractures.

2 MODEL DESCRIPTION

The diversity and variability of the geometry of a single, natural fracture and the complexity of the two-phase interaction and interference have made it difficult to reach a unique and accurate model to describe the two-phase flow behavior by means of the relative permeability concept. With the development of the visualization and surface measurement techniques, it has become possible to observe the multiphase flow behavior dynamically and to quantify the geometrical heterogeneity in fracture space. Nicholl et al. (2000) studied the effect of the immobile phase on the flowing-phase relative permeability in the satiated condition and developed a conceptual model for flowing-phase relative permeability by using the effective medium approach suggested by Zimmerman and Bodvarsson (1996). In the conceptual model of Nicholl et al. (2000), an in-place tortuosity induced by the immobile phase was used as a correction term to decrease the effective hydraulic gradient. The flowing-phase (water) relative permeability is then obtained as:

$$k_{rw} = S_w \tau_{ip} \underbrace{\left[\frac{\langle b_f \rangle^2}{\langle b \rangle^2} \right] \left[\left(1 + \frac{9\sigma_b^2}{\langle b \rangle^2} \right)^{1/2} \left(1 + \frac{9\sigma_{bf}^2}{\langle b_f \rangle^2} \right)^{-1/2} \right]}_{A} \quad (1)$$

where k_{rw} and S_w are the wetting-phase (water) relative permeability and saturation respectively, $\langle b \rangle$ and σ_b^2 are the mean and variance of the aperture field, the subscript $(_f)$ refers to parameters for the region occupied by the flowing phase, and τ_{ip} (range from 0 to 1) is the in-place tortuosity. From their definition, the smaller the value of τ_{ip}, the more tortuous the flowing phase structure behaves. Since their

experiment was conducted in the satiated condition, nonwetting (air) phase remained entrapped. Nonwetting relative permeability was therefore always zero. From the experimental data, Nicholl et al. (2000) concluded that the in-place tortuosity is the dominant factor controlling the flowing phase relative permeability. However, the in-place tortuosity could not be measured in their study. Instead, in-place tortuosity was estimated independently by further simulating flow on the measured phase geometries under some simplified assumptions.

Chen et al. (2004a) conducted drainage (nonwetting phase displaces wetting phase) air-water cocurrent flow experiments in a smooth-walled fracture and defined a similar but measurable tortuosity coefficient for the channel flow regime, called channel tortuosity; τ_c, and used this coefficient to characterize the morphology of flow structures. The definition of this apparent parameter is based on the area of the channel and the smallest bounding rectangle that covers the whole channel for a specific phase. By using digital video recording and image-processing techniques, thousands of continuous flow images were analyzed automatically, and different flow structures were recognized and separated. It was found that the channel flow was the major flow structure spanning most of the water saturation (S_w) range, except for extremely small or large values of S_w. The channel area, A_c, length and width of the smallest bounding box, L_x and L_y, were computed for channels of each phase. The channel tortuosities for gas and water were then defined as:

$$\tau_{c,g} = (\frac{L_x L_y}{A_c})_g \quad \text{and} \quad \tau_{c,w} = (\frac{L_x L_y}{A_c})_w \qquad (2)$$

where the subscripts ($_g$) and ($_w$) denote the gas and water phases respectively.

The detailed methodology and an illustration of the computation of τ_c can be found in Chen et al. (2004a). Similar to the definition in porous media, the coefficient τ_c for each phase varies from 1 to infinity, with the two end cases representing respectively a homogeneous straight channel (no dispersed phase) and an extremely tortuous channel for each phase. This coefficient is related to the interfacial area and, consequently, allows quantification of the shear stress at the interface between the two fluids. From the experimental data, Chen et al. (2004a) found that the coefficients of channel tortuosity dominate the reduction of relative permeability in comparison to the X-curve, and that the following relative permeability relationship could replicate the experimental data with good accuracy:

$$k_{rw} = \frac{S_w}{\tau_{c,w}} \qquad (3)$$

$$k_{rg} = \frac{S_g}{\tau_{c,g}} \qquad (4)$$

It is worth noting that because of their different definitions of the tortuosity, the τ_{cw} in Equation (3) and τ_{ip} in Equation (1) should be close to reciprocal. Therefore, for smooth-walled fractures ($\langle b \rangle = \langle b_f \rangle$ and $\sigma_b^2 = \sigma_{bf}^2$), and Equation (1) can be simplified to Equation (3).
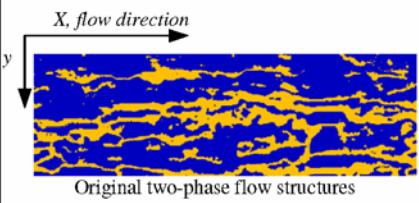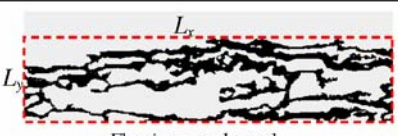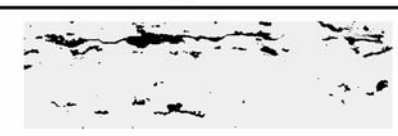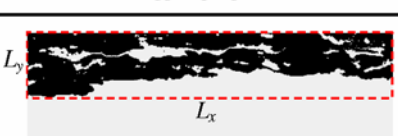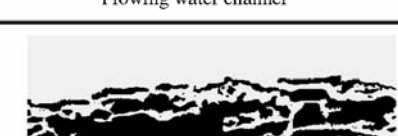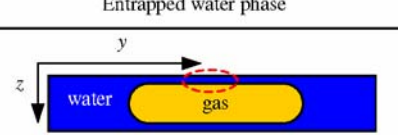

	Separated structures (in dark color)	Major impact	Included terms
Original two-phase flow structures	Flowing gas channel	• Gas rates • Gas tortuosity	$\tau_{c,g}$
	Entrapped gas phase	• Water tortuosity	$\tau_{c,w}$
	Flowing water channel	• Water rates • Water tortuosity	$\tau_{c,w}$
	Entrapped water phase	• Gas tortuosity • Immobile water saturation	$\tau_{c,g}$ S_{wr}
	Water film flow	• Gas rates • Water rates	F_m

Figure 1: Illustration of separating the two-phase flow structures and the major impact parameters in each separated structure considered in the rough-walled TCA for drainage process.
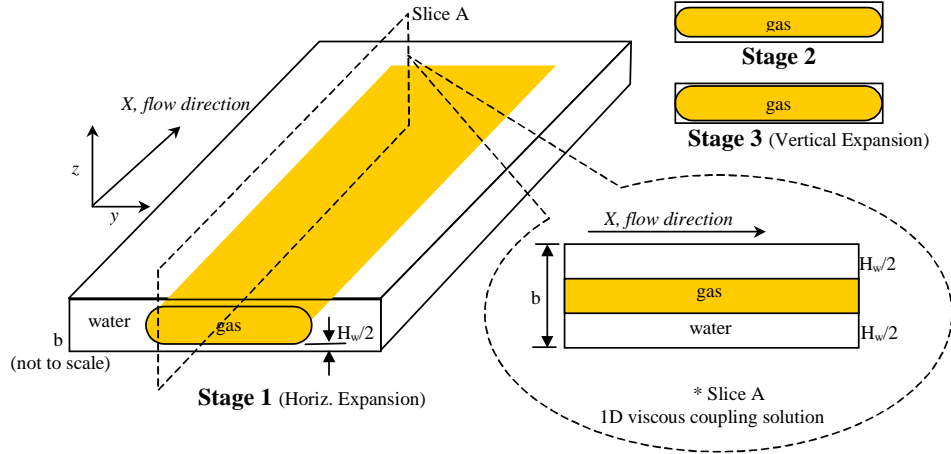
Figure 2: A simple superposition method for integrating one-dimensional viscous coupling model to two-dimensional viscous coupling model. The water film thickness, H_w, was assumed being constant during stage 1 and 2. After Stage 2, the H_w starts decreasing and the corresponding relative permeabilities approximately follows one-dimensional viscous coupling. (b and H_w are not to scale)

For the drainage relative permeabilities in rough-walled fractures, a major factor that was not considered in Equations (3) and (4) was the residual water, which was observed to be negligible in the smooth-walled case. The significant capillary force due to local aperture field variation can entrap considerable amounts of water phase, and some of it will contribute to the residual water saturation (S_{wr}) ultimately. To this end, a more rigorous approach by separating different phase structures was developed. Figure 1 illustrates the principle and concepts of this rough-walled tortuous channel approach. The two-phase flow structures were separated into three major parts, namely the flowing channels, the entrapped phases and the water film flowing along the fracture surfaces. During the steady-state drainage process, the first two parts were fully or partially included in the channel tortuosity terms, except for the considerable immobile and residual water phase. In analogy to earlier studies of relative permeability modeling in porous media (Brooks and Corey, 1966; van Genuchten, 1980), the immobile and residual phases were taken into account by normalizing the water saturation. For the drainage process, the normalized water saturation is:

$$S_w^* = \frac{S_w - S_{wr}}{1 - S_{wr}} \qquad (5)$$

where subscript (${}_r$) refers to residual saturation.

Regarding the water film flow along the fracture surfaces, an extended two-dimensional viscous coupling model was used to evaluate the effect of film thickness on relative permeabilities. The one-dimensional viscous coupling model was obtained by integrating Stoke's equations under parallel-plate assumption. The one-dimensional model was then defines as:

$$k_{rw} = \frac{S_w^2}{2}(3 - S_w) \qquad (6)$$

$$k_{rg} = (1 - S_w)^3 + \frac{3}{2}\mu_r S_w (1 - S_w)(2 - S_w) \qquad (7)$$

where $\mu_r = \mu_g/\mu_w$ is the viscosity ratio.

Since the one-dimensional viscous coupling model has poor representation of the real two-phase flow behaviors in fractures, the simplified but more practical geometrical consideration of the drainage process in an ideal fracture space is shown in Figure 2. The gas channel was initially assumed to be in a round-ended rectangular column with constant height, H_w, which is close to but always smaller than the fracture aperture, b. The relative permeability was computed by using either the superposition or integration of the one-dimensional solution in each vertical slice as shown in Figure 2. After the gas channel reaches the fracture boundaries (Stage 2), the gas phase starts to expend vertically and the corresponding relative permeability approximately follows one-dimensional viscous coupling in Stage 3. By setting different values of the water film ratio, H_w/b, and assuming the fracture width was much larger than its aperture, the effect of water film thickness on air-water relative permeabilities is shown in Figure 3. The water film ratio affects the relative permeabilities almost linearly because the scale of the fracture aperture is relatively small. In addition, the effect on gas-phase relative permeabilities is stronger than on the water phase. Consequently, film flow correctors, F_{mw} and F_{mg}, were suggested as corrections to the relative permeabilities to account for the water film flow. Combining all factors in Figure 1, the modified TCA for describing the relative permeabilities of the rough fractures can be written in the following form:

$$k_{rw} = \frac{S_w^*}{\tau_{c,w}} F_{mw} \qquad (8)$$

$$k_{rg} = \frac{S_g}{\tau_{c,g}} F_{mg} \qquad (9)$$

Comparing Equation (8) to Equation (1) and examining the definition of the channel tortuosities, we can see that part A in Equation (1) has inherently contributed to the coefficients of $\tau_{c,w}$, and S_w^*.

Generally, the water film in partially saturated rock surfaces is attributed to adsorptive forces on flat surfaces of minerals or by capillary effects within the surface roughness. The metric potential is the major parameter that controls the

thickness of the film. By considering the fracture-matrix interaction in fractured porous media, Tokunaga and Wan (1997) measured average surface film thickness ranging from 2 to 70 μm. However, for a single fracture with an impermeable matrix as in our cases, earlier studies indicated that the water film ratio was less than 1% (Romm, 1966; Pan et al., 1996) for smooth-walled fractures. However this ratio may increase for the rough-walled fractures since surface roughness and pits on the surface increase capillary and absorption forces. To the best of our knowledge, no practical methods exist to estimate the H_w in accordance with different surface geometry for a single fracture with impermeable surfaces. Judging from the study by Romm (1966) and the corresponding result in Figure 3, the water film ratio should be small and F_m should be close to 1, which means that the film effect on the relative permeabilities may be insignificant. Following this result, Equations (8) and (9) can be further simplified to:

$$k_{rw} = \frac{S_w^*}{\tau_{c,w}} \tag{10}$$

$$k_{rg} = \frac{S_g}{\tau_{c,g}} \tag{11}$$

In these simple equations, only two measurable parameters are needed. The residual saturation is readily obtained in the laboratory; however, the channel tortuosity has to be obtained by the aid of tomography or visualization techniques during two-phase flow experiments, unless some correlation between channel tortuosities and fracture geometry can be built to predict the channel tortuosity. To this end, several experiments were conducted to explore this issue and verify the model.
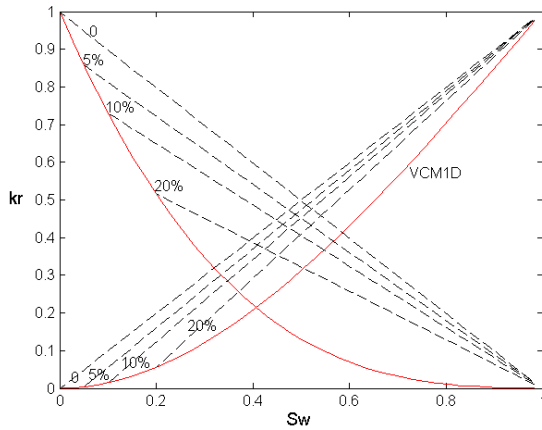

Figure 3: Effect of water film thickness on air-water relative permeabilities. VCM1D is the one-dimensional viscous coupling model. The percentage means the water film ratio (H_w/b).

3 EXPERIMENTS

The fractures for the experiments were made by transparent silica glass with dimensions around 30cm (L) x 10cm (W). Two fractures with distinct surface roughness, randomly rough (RR) and homogeneously rough (HR) fractures, were used in the steady-state air-water cocurrent drainage experiments to represent two distinct surface geometries and heterogeneities. The experiment of the RR case was conducted during this study while the data from the HR case were provided by an earlier experiment (Chen et al. 2004b). Details of the experimental apparatus and procedures can be

found in Chen et al. (2004a). The three-dimensional profile of the RR fracture and the two-dimensional suface pattern of the HR fracture are shown in Figure 4. The RR fracture has a hydraulic aperature of around 240 μm (~4800 darcy in permeability). The three-dimensional surface profile was measured by Leitz PMM 12106 CMM Stylus Machine (20 microns resolution, ~2 microns precision). The HR fracture has repeatable wedge-shaped pattern with hydraulic aperature of around 145 μm (~1750 darcy in permeability).
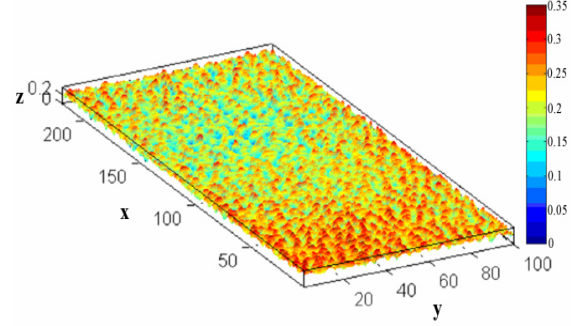
(a) Randomly rough fracture (Max. aperature variation ~ 350 μm)
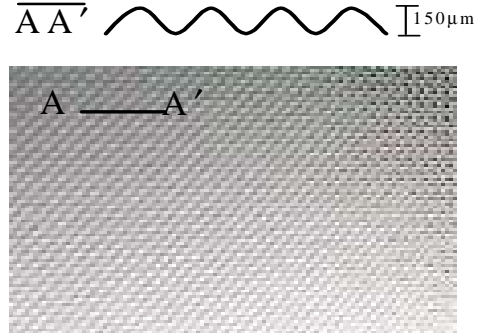
(b) Homogeneously rough fracture (Max. aperature variation ~ 150 μm)

Figure 4: Surface profile of the rough-walled fractures: (a) three-dimensional profile of the RR fracture; (b) two-dimensional suface pattern of the HR fracture.

Initially, the fractures were fully saturated with deionized water. The drainage process was controlled by adjusting water and gas injection rates to decrease the water sturation. First, the water rate was kept constant while increasing gas rate to decrease the water saturation through the fracture until the water saturation was no longer sensitive to the increase of the gas rates. Then, the water rate was decreased further and the previous procedure was repeated. To avoid the dissolution of the gas phase and evaporation of the water phase, the water was equilibrated with air and the nirogen gas was saturated with water-vapor. During each designated input rate of gas and water, the data were acquired when a stable or repeatable flow structure had been reached. After finishing one run (one pair of prescribed water and gas rates), the flow structures were destroyed by rapidly flushing water through the fractures, and then another run was commenced.

According to air-water experiments reported by earlier studies (Persoff and Pruess, 1995; Diomampo, 2001; Chen et al. 2004a), the fracture flow experiments are unsteady by nature. While input rates of water and gas were fixed,

considerable pressure fluctuations accompanied by corresponding saturation changes occurred, which made flow rates through the fractures vary. A traditional time-average data processing was deemed to be infeasible and unrepresentative since every datum fluctuation may indicate a corresponding fluctuation of flow structure and saturation. To overcome these issues, all instantaneous data were acquired in a period less than or equal to one second. The high-speed data acquisition system gathered instantaneous pressure and flow rate, while instantaneous gathering of saturation and flow structure data was accomplished by the use of the digital video camcorder and automatic image processing techniques.

4 RESULTS AND DISCUSSION

Around 3000 data points were obtained in each experiment within a period of 1 second. The information of pressure, rates and saturation were then used to compute relative permeabilities using generalized two-phase Darcy equations. These experimental results served as the reference relative permeabilities to validate the suggested model (Equations (10) and (11)). Continuous flow images from these experiments were analyzed. Phase channels were recognized, and the $\tau_{c,w}$ and $\tau_{c,g}$ values were then computed. Figure 5 shows several representative images extracted from these two experiments as well as the smooth-walled images replicated from Chen et al. (2004a). Snapshots in each row in Figure 5 have similar water saturation but are from different type of fractures. Clearly, the channel tortuosity increases when the heterogeneity of the fracture surface increases. The phase channels in RR fracture are always the most tortuous among these three cases. In general, for a specific fracture, the channel tortuosity of one phase has a countertrend to the saturation of that phase. In other words, the water (gas) channel tortuosity increases when the water

(gas) saturation decreases. With increasing surface heterogeneity, the nested behavior of flow structures was increasingly apparent. Even though the flow structures were destroyed before changing the input rates, the gas phase had some stationary preferential pathways in the rough fractures, particularly in the RR fracture. When the gas saturation increased further, the gas channels expanded from these base pathways or branched from them. This behavior may demonstrate the likely flow structure evolution in natural fractures.

After analyzing thousands of images, the channel tortuosities of each phase were evaluated, and then the relative permeabilities were computed using the proposed TCA in Equations (10) and (11). Figures 6 and 7 compare these results to the reference experimental relative permeabilities from the generalized Darcy equations for the RR and FR fractures respectively. Due to the unstable nature of the flow, the experimental relative permeabilities are scattered. For the RR fracture, the result from TCA fits the experimental result with good accuracy. The gas-phase relative permeabilities seem to be overestimated slightly. Close agreement was also obtained in the HR fracture case. However, the gas-phase values from TCA were larger than the experimental result. The overestimation in gas-phase relative permeability may be attributed to the water film flow effect as demonstrated in the previous section (but neglected in the current study), or the experimental and image processing errors. The major source of the image processing errors was from the recognition of the channel connectivity, particularly for the rough-walled fractures. Because of the local aperture variation, some phase channels were connected via thin threads that were too narrow to be recognized in the images in a few cases. This led to the less accurate calculation of tortuosity.

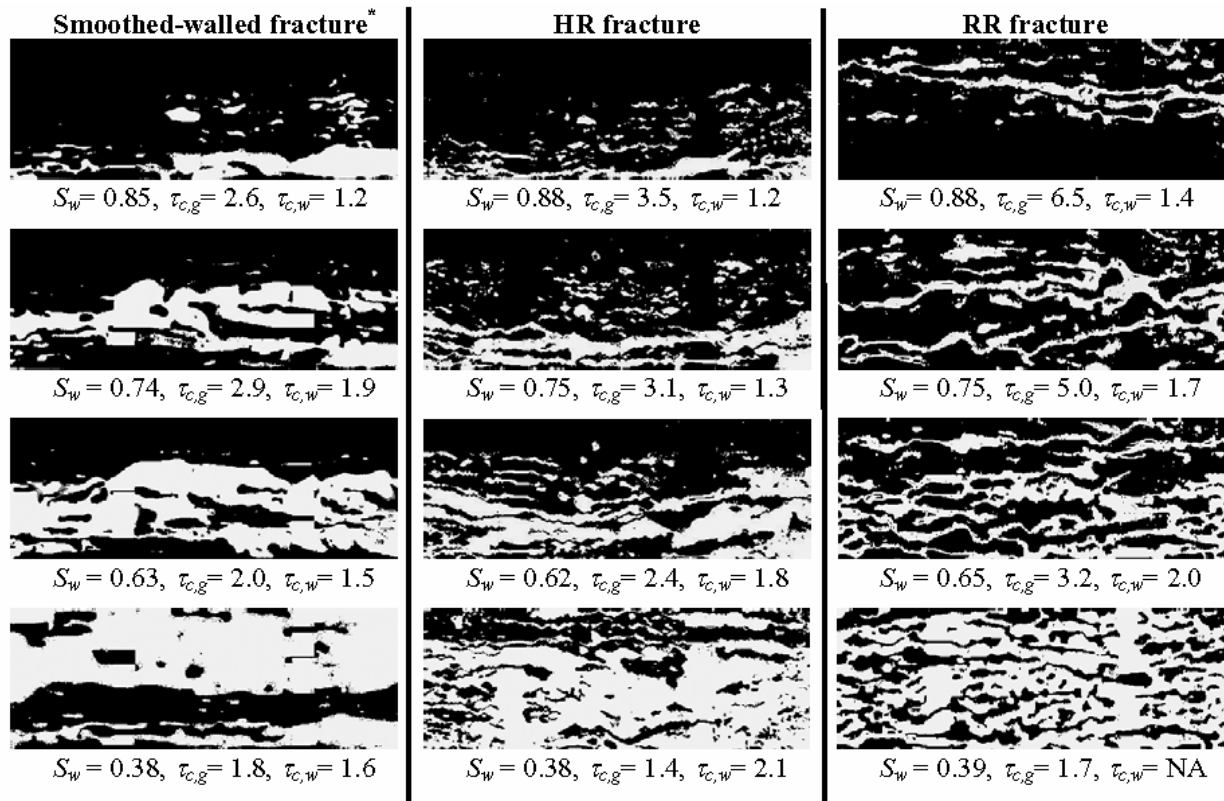| Smoothed-walled fracture[*]	HR fracture	RR fracture
$S_w = 0.85$, $\tau_{c,g} = 2.6$, $\tau_{c,w} = 1.2$	$S_w = 0.88$, $\tau_{c,g} = 3.5$, $\tau_{c,w} = 1.2$	$S_w = 0.88$, $\tau_{c,g} = 6.5$, $\tau_{c,w} = 1.4$
$S_w = 0.74$, $\tau_{c,g} = 2.9$, $\tau_{c,w} = 1.9$	$S_w = 0.75$, $\tau_{c,g} = 3.1$, $\tau_{c,w} = 1.3$	$S_w = 0.75$, $\tau_{c,g} = 5.0$, $\tau_{c,w} = 1.7$
$S_w = 0.63$, $\tau_{c,g} = 2.0$, $\tau_{c,w} = 1.5$	$S_w = 0.62$, $\tau_{c,g} = 2.4$, $\tau_{c,w} = 1.8$	$S_w = 0.65$, $\tau_{c,g} = 3.2$, $\tau_{c,w} = 2.0$
$S_w = 0.38$, $\tau_{c,g} = 1.8$, $\tau_{c,w} = 1.6$	$S_w = 0.38$, $\tau_{c,g} = 1.4$, $\tau_{c,w} = 2.1$	$S_w = 0.39$, $\tau_{c,g} = 1.7$, $\tau_{c,w} = NA$

Figure 5: Representative images extracted from the image-processing program of channel recognition for the smooth and rough fractures and corresponding channel tortuosities evaluated. (Gas phase is white and water is black. [*]Smooth-walled images are from Chen et al., 2004a)
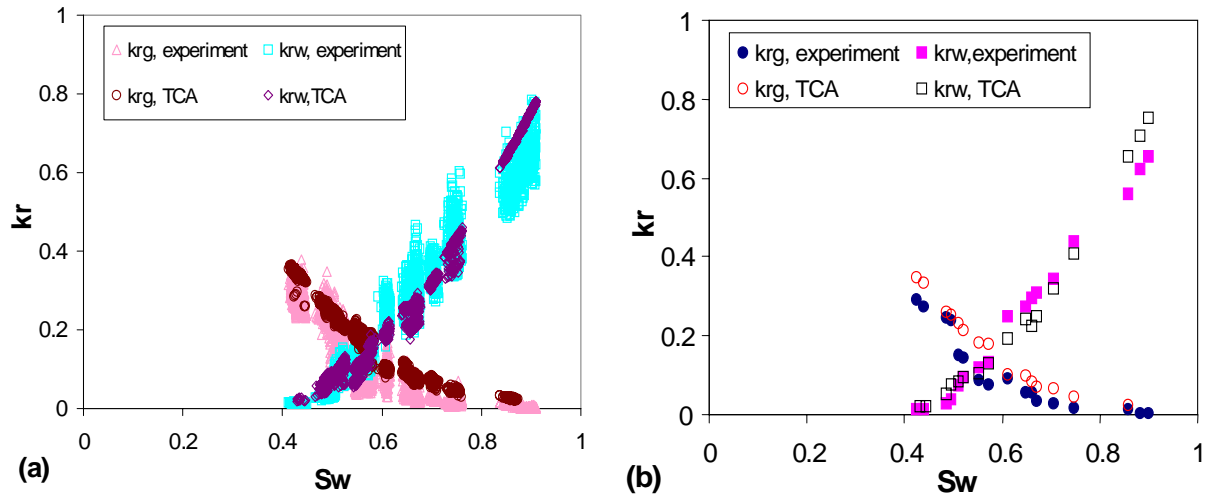
Figure 6: Relative permeabilities from tortuous-channel approach and its comparison with the experimental result for the RR fracture: (a) all data points (~3000 points), (b) averages of each runs in (a).
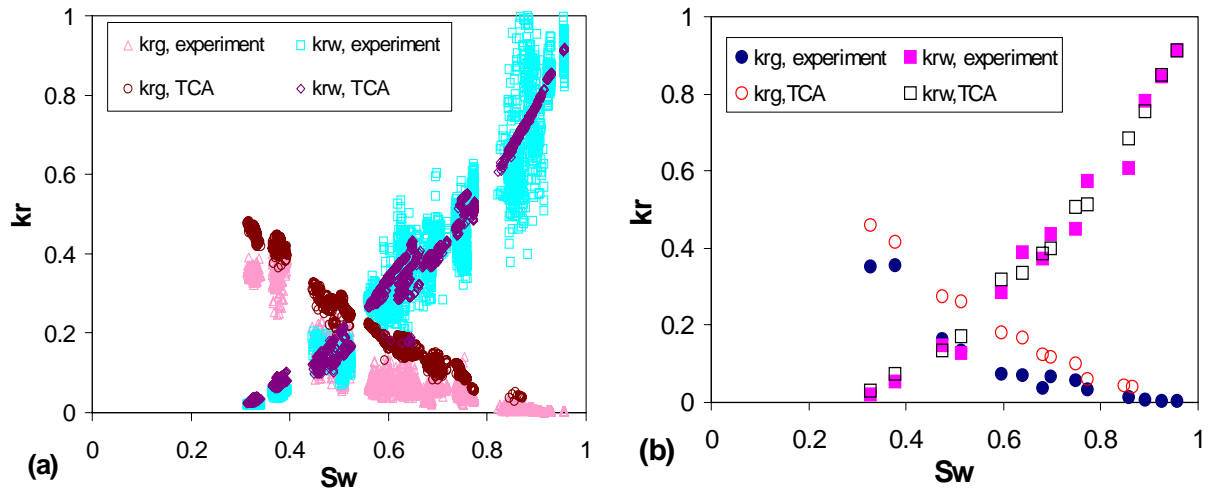

Figure 7: Relative permeabilities from tortuous-channel approach and its comparison with the experimental result for the HR fracture: (a) all data points (~3000 points), (b) averages of each runs in (a).
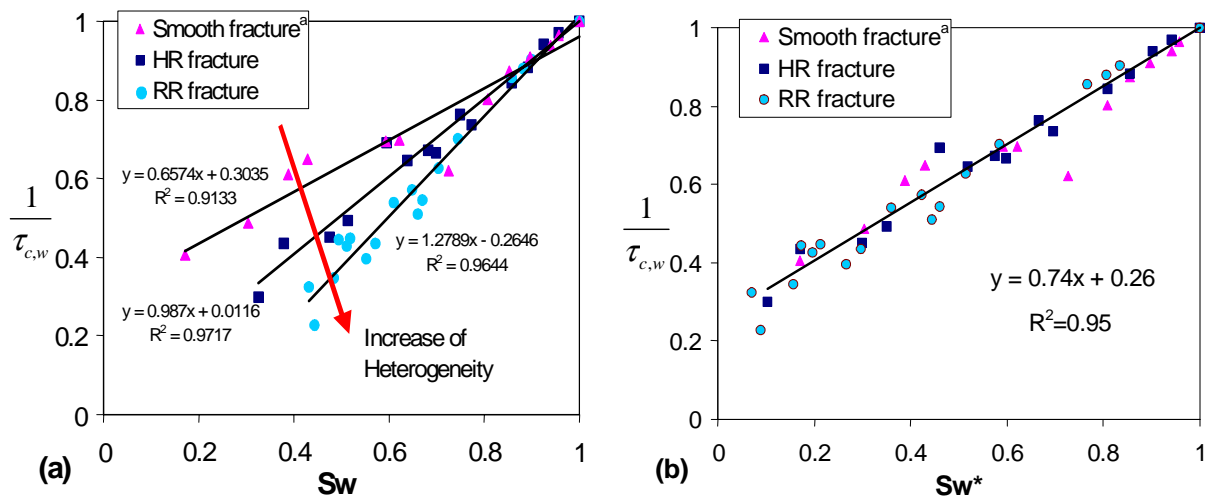

Figure 8: Reciprocal of average water channel tortuosity versus (a) water saturation and (b) normalized water saturation for smooth and rough fractures. ([a]: from Chen et al., 2004a)

The evolution of phase channels shown in Figure 5 may reveal the correlation between the channel tortuosity and the surface geometry and heterogeneity of fractures. Earlier studies also suggested that relative permeabilities in fractures are sensitive to the nature and range of spatial correlation between apertures (Pruess and Tsang, 1990). Combining current results with the smooth-walled results from Chen et al. (2004a), Figure 8a shows the reciprocal of average water-phase tortuosity versus water saturation for all of the fractures studied. A straight channel has a value of reciprocal of tortuosity equal to 1. As can be seen in this figure, acceptable linear trends can be found in these three cases, while their slopes increase when the heterogeneity of the fracture surfaces increases. Interestingly, these data seem to collapse to a single linear trendline when plotted in normalized water saturation as shown in Figure 8b. On the other hand, the average gas channel tortuosities show similar trends in the smooth and the HR fractures while the RR fracture results demonstrate a slightly more tortuous trend as shown in Figure 9. However, most of the deviated points in Figure 9 were close to the end point of the gas saturation, which has a less significant inference on the Equations (10) and (11). All of these gas-phase tortuosities can be expressed approximately in a second-order relationship with respect to gas saturation.
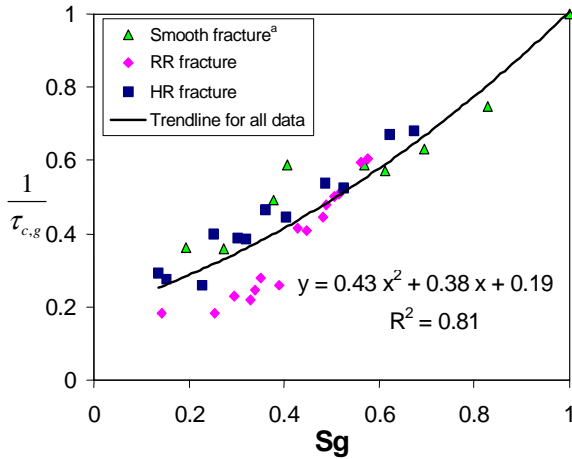

Figure 9: Reciprocal of average gas channel tortuosity versus gas saturation for smooth and rough fractures. ([a]: from Chen et al., 2004a)

Generalizing from these three specific types of fractures, preliminary and empirical correlation equations between the channel tortuosity and saturation can be obtained as shown in Figures 8b and 9. Substituting these equations into Equations (10) and (11), the tortuous channel model (TCM) for the three fractures we studied is then obtained as:

$$k_{rw} = 0.74 S_w^{*2} + 0.26 S_w^* \qquad (12)$$

$$k_{rg} = 0.43 S_g^3 + 0.38 S_g^2 + 0.19 S_g \qquad (13)$$

Fitting this model to the experimental results is shown in Figure 10. Close agreement was obtained between this tortuous channel model and the experimental measurements. Using measured values of residual water saturation S_{wr} from the experiments of the rough fractures, this model can describe the water-phase relative permeabilities with good accuracy, accounting for the residual phase. The gas-phase curve generalized from all gas-phase tortuosities seems to overestimate k_{rg} slightly compared to the experimental

result; nevertheless the model curve can still capture the trend of the experimental data.
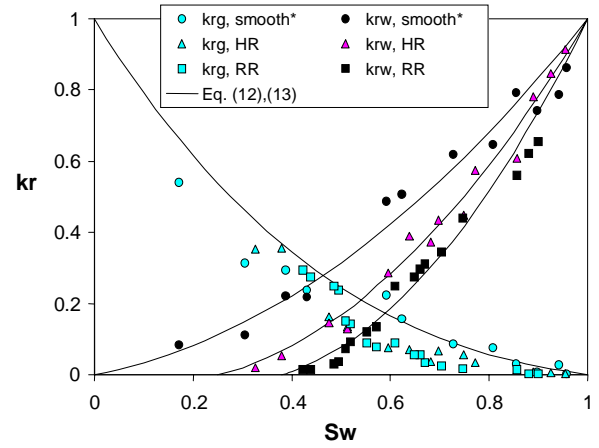

Figure 10: Comparison of the experimental relative permeabilities with the TCM using Equations (12) and (13) for the smooth-walled, HR and RR fractures. The S_{wr} for HR and RR fractures is 0.25 and 0.39 respectively determined from the experiments. ([*]: from Chen et al., 2004a)
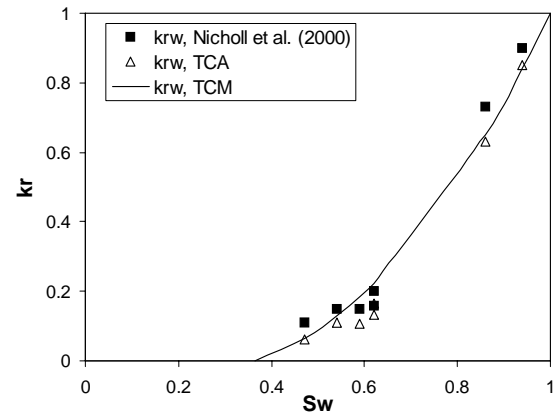

Figure 11: Using proposed TCA and TCM to interpret flowing-phase relative permeabilities from Nicholl et al. (2000) by setting S_{wr} = 0.36.
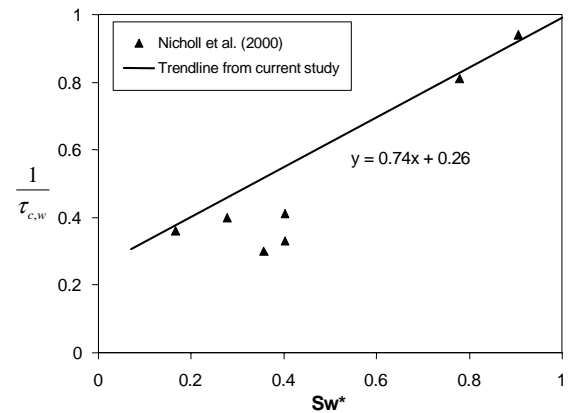

Figure 12: Plot of reciprocal of in-place tortuosities from Nicholl et al. (2000) versus normalized water saturation by setting S_{wr} = 0.36.

Nicholl and Glass (1994) conducted experiments to measure flowing-phase (water phase) relative permeabilities in the

presence of entrapped gas phase in a homogeneous, isotropic fracture. The corresponding in-place tortuosities were inferred from simulated flow rates using measured phase geometries (Nicholl et al., 2000). Although their experiments were conducted in satiated condition (water was the only flowing phase) and the final residual water saturation was not reported, Equation (10) still shows an acceptable fit to their flowing relative permeabilities by using their simulated tortuosities and setting a reasonable value for S_{wr} (0.36), as illustrated in Figure 11. In addition, most of the simulated tortuosities fall on the linear trendline suggested in this study (Figure 12). Pruess and Tsang (1990) predicted fracture relative permeabilities from numerical simulation of conceptual and heterogeneous fracture geometries. The phase occupancy and permeability were derived by assuming a parallel-plate model for small subregions in the fracture plane. Although only qualitative applications were suggested and the nonwetting phase relative permeabilities were deemed to be less physical in their simulated results, the wetting–phase relative permeabilities did follow a conventional pattern. As shown in Figure 13, these numerical results can be interpreted by the proposed tortuous channel model by setting a reasonable value for S_{wr}.
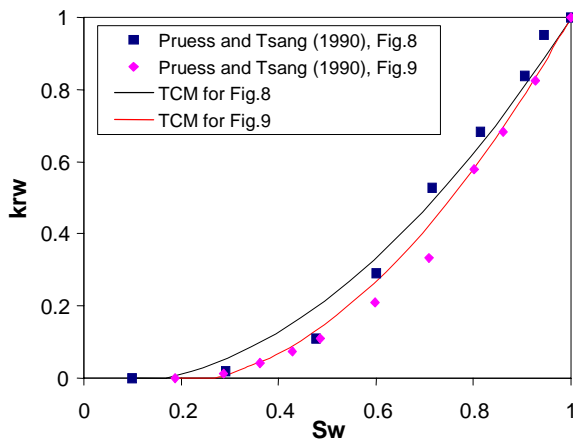

Figure 13: Using proposed tortuous channel model (Equations (12) and (13)) to interpret the water-phase relative permeabilities from earlier numerical study done by Pruess and Tsang (1990). (S_{wr} was set to be 0.27 and 0.17 respectively)

5 CONCLUSIONS

This study has demonstrated the possibility of using a flow-structure model to predict the corresponding relative permeabilities in rough-walled fractures. The proposed approach can represent the experimental data from current and earlier studies with good agreement. By studying three fractures with different surface roughness, we found that the magnitude of the flow channel tortuosity increases when the heterogeneity of fracture surface increases. Generalizing from all the channel tortuosities measured in these three fractures, we suggested an empirical, tortuous channel model. Although some successful descriptions of relative permeabilities in rough-walled fractures using the proposed tortuous channel approach and model were achieved, it is very important to emphasize the limitations. At this moment, the method of evaluating the coefficient of tortuosity and the feasibility of using the tortuous-channel approach were only validated in specific artificial fractures made of silica glass. To account for the complex connectivity and flow structures in full-scale naturally-fractured media, the algorithm to evaluate τ_c and the methodology to characterize the flow-

based heterogeneity may have to be developed further. Characterizing the flow-based heterogeneity of the fractures is believed to be the major challenge of the future application. The tortuous-channel model (Equations (12) and (13)) was developed from current results empirically. The characteristics of heterogeneity in natural fractures are certainly much more complex and variable. Therefore more studies of the relationship between tortuosity and fracture geometry may be needed to gain rigorous models for predicting fracture relative permeabilities accurately. If such work can be achieved, perhaps the relative permeabilities of natural fractures can be predicted simply by measuring S_{wr} and the geometry of the fracture surface or by using tomographic technology to determine channel tortuosity.

REFERENCES

Brooks, R.H. and Corey, A.T.: "Properties of Porous Media Affecting Fluid Flow," *J. Irrig. And Drain. Div.*, Proc. ASCE, IR2 (1966), Vol. 92, p. 61-88.

Chen, C.-Y., Horne, R.N., and Fourar, M.: "Experimental Study of Liquid-Gas Flow Structure Effects on Relative Permeabilities in a Fracture," *Water Resources Research*, (Aug 2004a), Vol. 40, No.8, W08301.

Chen, C.-Y., Li, K., and Horne, R.N.: "Experimental Study of Phase Transformation Effects on Relative Permeabilities in Fractures," paper SPE 90233, presented in SPE 2004 Annual Technical Conference and Exhibition, Houston, TX, USA, September.26-29, 2004b.

Diomampo, G.P.: *Relative Permeability through Fractures*, MS thesis, Stanford University, Stanford, California (2001).

Lomize, G.M.: *Flow in Fractured Rocks,* (Gosenergoizdat, Moscow, 1951).

Meheust, Y., Schmittbuhl, J.: "Geometrical Heterogeneities and Permeability Anisotropy of Rough Fractures," *Journal of Geophysical Research*, (Feb. 2001); Vol.106, No.B2, p.2089-2102.

Nicholl, M.J. and Glass, R.J: "Wetting Phase Permeability in A Partially Saturated Horizontal Fracture," Proc. 5th Ann. Int. Conf. On High Level Rad. Waste Mgmt., 2007-19, American Nuclear Society, Las Vegas, Nevada, May 22-26,1994.

Nicholl, M.J., Rajaram, H. and Glass, R.J.: "Factors Controlling Satiated Relative Permeability in a Partially Saturated Horizontal Fracture," *Geophysical Research Letters*, (Feb. 2000), Vol.27, No.3, p.393-396.

Pan, X., Wong, R.C. and Maini, B.B.: "Steady State Two-Phase Flow in a Smooth Parallel Fracture," presented at the 47th Annual Technical Meeting of the Petroleum Society in Calgary, Alberta, Canada, June 10-12, 1996.

Persoff, P. and Pruess, K.: "Two-Phase Flow Visualization and Relative Permeability Measurement in Natural Rough-Walled Rock Fractures," *Water Resources Research* (May 1995) Vol. 31, No. 5, p. 1175-1186.

Pruess, K. and Tsang, Y. W.: "On Two-Phase Relative Permeability and Capillary Pressure of Rough-Walled Rock Fractures," *Water Resources Research* (Sept. 1990) Vol. 26 No. 9, p. 1915-1926.

Romm, E.S.: *Fluid Flow in Fractured Rocks*, "Nedra" Publishing House, Moscow (Translated from the Russian) (1966).

Tokunaga, T.K. and Wan, J.M.: "Water Film Flow along Fracture Surfaces of Porous Rock," *Water Resources Research*, (Jun 1997), Vol.33, No.6, p.1287-1295.

van Genuchten, M.T.: "A Closed Form Equation for Predicting the Hydraulic Conductivity of Unsaturated Soils," *Soil Science Society of America Journal*, (1980), Vol.44, No.5, p.892-898.

Witherspoon, P.A., Wang, J.S.W., Iwai, K. and Gale, J.E.: "Validity of Cubic Law for Fluid Flow in a Deformable Rock Fracture," *Water Resources Research*, (1980), Vol. 16, No. 6, pp 1016-1024.

Zimmerman, R.W. and Bodvarsson, G.S.: "Hydraulic Conductivity of Rock Fractures," *Transport in Porous Media*, (Apr 1996), Vol.23, No.1, p.1-30.